NEUTRON STAR STRUCTURE AND NUCLEAR MATTER PROPERTIES FROM A GENERAL WALECKA-TYPE MODEL WITH BAYESIAN ANALYSIS*

Yao Ma

School of Frontier Sciences, Nanjing University, Suzhou 215163, China

Jia-Ying Xiong†

School of Frontier Sciences, Nanjing University, Suzhou 215163, China
and
School of Fundamental Physics and Mathematical Sciences
Hangzhou Institute for Advanced Study, UCAS
Hangzhou 310024, China

Received 27 March 2026, accepted 8 June 2026, published online 10 July 2026

We establish a Bayesian analysis framework with a general Walecka-type relativistic mean-field model to study dense nuclear matter under constraints from nuclear matter properties and neutron star observations. With the experimental and observational data well described, we find that pure hadronic descriptions can generate a peak structure in the sound velocity by ω, ρ, σ, and a_0 meson mixing, which is crucial for describing both medium and massive neutron stars. As the peak structure is frequently interpreted as a signature of phase transitions, our findings provide a new perspective on the microscopic origin of the sound-velocity peak just with pure hadronic matter.

DOI:10.5506/APhysPolBSupp.19.4-A12

1. Introduction

The discovery of GW170817 [1] from a binary neutron star inspiral, combined with electromagnetic observations, constrains neutron star (NS) structures such as mass–radius (M–R) relations, and tidal deformation. These relate to the equation of state (EOS) of nuclear matter (NM), allowing us to probe NM in extreme regimes, while nuclear experiments such as heavy-ion

* Presented at the Excited QCD 2026 Workshop, Granada, Spain, 8–14 January, 2026.

† Corresponding author: xiongjiaying21@mails.ucas.ac.cn

collisions and nuclei structure analysis constrain NM properties around saturation density. Theoretical developments such as Walecka-type relativistic mean-field (RMF) models [2] have made significant progress, but combining constraints from different sources remains challenging due to the complex interplay of nuclear forces and non-perturbative QCD.

We present an AI-driven Bayesian analysis platform to search for the optimal parameter space of a general Walecka-type RMF model [3, 4], incorporating all mesons lighter than 1 GeV with constraints from nuclei structures, heavy-ion collisions, and astrophysical observations. We find that pure hadronic descriptions can generate a peak structure in the sound velocity through ω, ρ, σ, and a_0 meson mixing, which is crucial for describing both medium and massive neutron stars, so that the optimal parameter space can simultaneously describe the NM properties around saturation density and NS structures.

2. The analysis framework

2.1. The Bayesian analysis framework and experimental constraints

The Bayesian analysis provides a systematic framework to incorporate various constraints from nuclear physics experiments and astrophysical observations based on Bayes' theorem

$$p(\boldsymbol{\theta} \mid \boldsymbol{D}) = \frac{p(\boldsymbol{D} \mid \boldsymbol{\theta}) p(\boldsymbol{\theta})}{p(\boldsymbol{D})}\,, \tag{1}$$

where $\boldsymbol{\theta}$ denotes the model parameters, $p(\boldsymbol{\theta})$ is the prior distribution, $p(\boldsymbol{D} \mid \boldsymbol{\theta})$ is the likelihood function, and $p(\boldsymbol{D})$ is the Bayesian evidence serving as a normalization constant

$$p(\boldsymbol{D}) = \int p(\boldsymbol{D} \mid \boldsymbol{\theta}) p(\boldsymbol{\theta}) \mathrm{d}\boldsymbol{\theta}\,. \tag{2}$$

With the assumption that the different data are conditionally independent, the overall likelihood factorizes as

$$p(\boldsymbol{D} \mid \boldsymbol{\theta}) = \prod_{i=1}^{n} p\left(D_i \mid \boldsymbol{\theta}\right)\,. \tag{3}$$

In this work, the data $\boldsymbol{D}$ consist of two parts: the NM properties and the M–R relations of neutron stars. The NM properties around saturation density n_0 include the binding energy $e(n)$, pressure $P(n)$, incompressibility $K(n)$, symmetry energy $E_{\mathrm{sym}}(n)$, and its slope $L(n)$, whose definitions can be found in Ref. [5]. Since these properties are derived from different theoretical models and experiments, we summarize them as reasonable ranges supported by current knowledge, each modeled as a normal distribution with

one standard deviation for simplicity. For the M–R relations, Refs. [1, 6–11] provide the corresponding regions, and the contribution of the M–R relation to Eq. (3) is estimated from the maximum value of the predicted M–R line for a given constraint.

2.2. A general Walecka-type model for dense nuclear matter

The model is a general Walecka-type RMF model incorporating the relevant degrees of freedom below 1 GeV, *i.e.*, the σ, ω, ρ, and a_0 mesons and the nucleons (n and p), with the π meson neglected in the RMF approximation; details can be found in Ref. [4]. The EOS and M–R relation are obtained from the RMF Hamiltonian and the Tolman–Oppenheimer–Volkoff equation, with computation methods given in Ref. [3], and the NS crust is interpolated to a BPS EoS [12, 13] below $0.5n_0$.

We fix the well-determined masses $m_\omega = 782$, $m_\rho = 763$, $m_{a_0} = 980$, and $m_N = 939$ MeV, while the less certain m_σ is varied from 400 to 800 MeV. The OBE couplings $g_{\sigma NN}$, $g_{\omega NN}$, $g_{\rho NN}$, and $g_{a_0 NN}$ are limited to $[-20, 20]$, and the magnitudes of the three- and four-meson couplings are taken to be below 10000 MeV and 1000, respectively (see Ref. [5] and references therein). The resulting 21 model parameters $\boldsymbol{\theta}$, from the Lagrangian of Ref. [4], make the evidence integral, Eq. (2), computationally challenging; we therefore adopt uniform priors within the above ranges and use Eq. (3) as the benchmark for the model performance.

3. Neutron star structure and sound velocity from the general Walecka-type model

With these constraints, we obtain two optimal parameter sets, GQHD1 and GQHD2, for the general Walecka-type model, whose details can be found in Ref. [4]. With well-reproduced NM properties, the resulting NS M–R relations, compared to past Walecka-type parameter sets, are shown in Fig. 1. One can see from Fig. 1 that, compared to past parameter sets, GQHD1 and GQHD2 perform better for the NS M–R relation in reproducing a more compact NS with mass around $1.4M_\odot$.

3.1. Sound velocity and the role of $\sigma\omega\rho a_0$ term

The speed of sound v_s^2 encodes the EOS stiffness and important aspects of QCD. While peak structures were previously attributed to phase transitions, Fig. 2 shows that GQHD1 and GQHD2 exhibit peaks at intermediate densities within pure hadronic matter. For GQHD1, v_s^2 becomes negative in the region $n_0 \lesssim n \lesssim 2n_0$ (Fig. 2), signaling a mechanical instability, before rising steeply to its peak near $2n_0$. Once the EOS reaches this unstable

region, it is truncated and extrapolated to the BPS crust EOS [12, 13]; the EOS actually used for the stellar structure is therefore mechanically stable ($v_s^2 \geq 0$) throughout, and the GQHD1 neutron-star sequence in Fig. 1 remains stable.

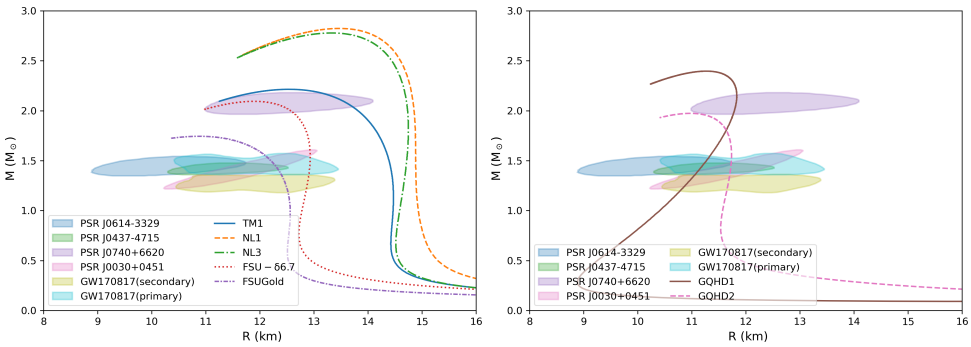

Fig. 1. The M–R relation for different parameter sets with beta equilibrium. The constraints PSR J1614-2230, PSR J0348+0432, PSR J0740+6620, J0030+0451, PSR J0437–4715, and PSR J0614–3329 are taken from Refs. [1, 6, 8–11, 14], respectively.

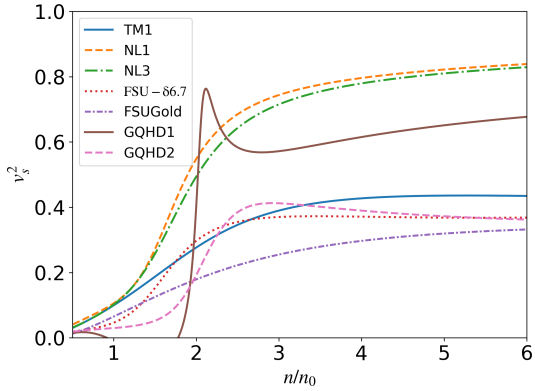

Fig. 2. Sound velocity v_s^2 *versus* density for various Walecka parameter sets [4, 15–19].

We found that the mixing term $b_8\sigma\omega\rho a_0$ is crucial for producing this peak. Figure 3 demonstrates that, as b_8 increases, the peak emerges and reduces NS radii around $1.4M_\odot$ while preserving the $2M_\odot$ constraint. Besides, at high densities, the GQHD2 v_s^2 approaches the conformal limit 1/3, while that of GQHD1 remains higher ($\gtrsim 0.6$) and does not reach this limit within the density range relevant to neutron stars (up to $6n_0$). This reflects a trade-off: GQHD1 is the parameter set we pick to reproduce a compact $1.4M_\odot$

star satisfying the constraint from PSR J0614–3329, and such a compact configuration requires a stiffer EOS at high densities, so that the approach of v_s^2 to the conformal limit is sacrificed; GQHD2, with a softer high-density EOS, instead approaches 1/3 but predicts a less compact star.

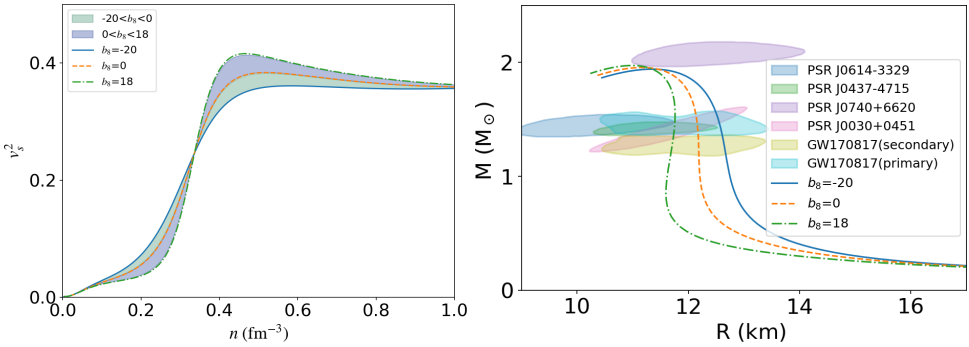

Fig. 3. Sound velocity and M–R relation for different b_8 values in GQHD2.

4. Summary and outlook

In this work, we developed a general Walecka-type RMF model for dense nuclear matter and performed a Bayesian analysis of its parameter space under constraints from NM properties and NS observations. The model includes operators that capture high-density behavior not considered in past studies; with an appropriate choice of parameters, it can produce a NS of mass $\sim 1.4M_\odot$ with a small radius compatible with PSR J0614–3329. The sound-velocity results demonstrate the role of the sound-speed peak in shaping NS structure and highlight the importance of the mixed interaction term $b_8\sigma\omega\rho a_0$ at intermediate densities, providing a new perspective on the microscopic origin of the peak within pure hadronic matter. In the future, we plan to extend our framework to NSs with chiral effective field theories [5], providing a clearer connection to the underlying QCD dynamics.

The work of Y.M. is supported by the Jiangsu Funding Program for Excellent Postdoctoral Talent under grant number 2025ZB516. The authors would like to thank for useful discussions with Dr. Ling-Jun Guo.

REFERENCES

[1] LIGO Scientific and Virgo collaborations (B.P. Abbott *et al.*), *Phys. Rev. Lett.* **119**, 161101 (2017).

[2] J.D. Walecka, *Ann. Phys.* **83**, 491 (1974).

[3] L.-J. Guo, J.-Y. Xiong, Y. Ma, Y.-L. Ma, *Astrophys. J.* **965**, 47 (2024).
[4] Y. Ma, Y.-L. Ma, J.-Y. Xiong, arXiv:2603.01933 [nucl-th].
[5] Y. Ma, Y.-L. Ma, *Phys. Rev. D* **112**, 054026 (2025).
[6] LIGO Scientific and Virgo collaborations (B.P. Abbott *et al.*), *Phys. Rev. Lett.* **121**, 161101 (2018).
[7] J. Antoniadis *et al.*, *Science* **340**, 6131 (2013).
[8] T. Salmi *et al.*, *Astrophys. J.* **974**, 294 (2024).
[9] S. Vinciguerra *et al.*, *Astrophys. J.* **961**, 62 (2024).
[10] D. Choudhury *et al.*, *Astrophys. J. Lett.* **971**, L20 (2024).
[11] L. Mauviard *et al.*, *Astrophys. J.* **995**, 60 (2025).
[12] G. Baym, C. Pethick, P. Sutherland, *Astrophys. J.* **170**, 299 (1971).
[13] W.D. Arnett, R.L. Bowers, *Astrophys. J. Suppl.* **33**, 415 (1977).
[14] LIGO Scientific, Virgo, Fermi GBM, INTEGRAL, IceCube, AstroSat Cadmium Zinc Telluride Imager Team, IPN, Insight-Hxmt, ANTARES, Swift, AGILE Team, 1M2H Team, Dark Energy Camera GW-EM, DES, DLT40, GRAWITA, Fermi-LAT, ATCA, ASKAP, Las Cumbres Observatory Group, OzGrav, DWF (Deeper Wider Faster Program), AST3, CAASTRO, VINROUGE, MASTER, J-GEM, GROWTH, JAGWAR, CaltechNRAO, TTU-NRAO, NuSTAR, Pan-STARRS, MAXI Team, TZAC Consortium, KU, Nordic Optical Telescope, ePESSTO, GROND, Texas Tech University, SALT Group, TOROS, BOOTES, MWA, CALET, IKI-GW Follow-up, H.E.S.S., LOFAR, LWA, HAWC, Pierre Auger, ALMA, Euro VLBI Team, Pi of Sky, Chandra Team at McGill University, DFN, ATLAS Telescopes, High Time Resolution Universe Survey, RIMAS, RATIR, SKA South Africa/MeerKAT collaborations (B.P. Abbott *et al.*), *Astrophys. J. Lett.* **848**, L12 (2017).
[15] Y. Sugahara, H. Toki, *Nucl. Phys. A* **579**, 557 (1994).
[16] P.-G. Reinhard *et al.*, *Z. Physik A — Atomic Nuclei* **323**, 13 (1986).
[17] G.A. Lalazissis, J. Konig, P. Ring, *Phys. Rev. C* **55**, 540 (1997).
[18] F. Li *et al.*, *Astrophys. J.* **929**, 183 (2022).
[19] B.G. Todd-Rutel, J. Piekarewicz, *Phys. Rev. Lett.* **95**, 122501 (2005).